ChemComm

COMMUNICATION

View Article Online
View Journal | View Issue

Cite this: *Chem. Commun.*, 2019, **55**, 2174

Received 3rd December 2018,
Accepted 22nd January 2019

DOI: 10.1039/c8cc09618j

rsc.li/chemcomm

Room temperature, liquid-phase Al_2O_3 surface coating approach for Ni-rich layered oxide cathode material†

Sven Neudeck,‡[a] Florian Strauss,‡[a] Grecia Garcia,[a] Hannes Wolf,[b] Jürgen Janek,[ac] Pascal Hartmann*[ab] and Torsten Brezesinski*[a]

A room temperature, atomic-layer-deposition-like coating strategy for NCM811 (80% Ni) is reported. Trimethylaluminum is shown to readily react with adsorbed moisture, leading both to Al_2O_3 surface layer formation on NCM811 and to trace H_2O removal in a single treatment step. Even more importantly, the cycling performance of pouch cells at 45 °C is greatly improved.

Layered lithium transition-metal oxides containing Co, Ni and Mn or Al such as $Li_{1+x}(Ni_{1-y-z}Co_yMn_z)_{1-x}O_2$ (NCM) and $LiNi_{0.80}Co_{0.15}Al_{0.05}O_2$ (NCA) are widely used as cathode active materials (CAMs) in lithium-ion batteries (LIBs) for electric vehicles.[1] Increasing the nickel content in the CAM leads to usable specific capacities of >200 mA h g^{-1}, and compositions such as $LiNi_{0.6}Co_{0.2}Mn_{0.2}O_2$ (NCM622) and $LiNi_{0.8}Co_{0.1}Mn_{0.1}O_2$ (NCM811) have already been commercialized for high-energy-density LIB applications.[2–5] However, it also adversely affects the cycling and thermal stability, thus calling for strategies to improve them further. A variety of surface functionalization and bulk doping routes have been reported to date, mainly aiming at mitigating the CAM degradation (*i.e.*, corrosion, leaching, self-pulverization *etc.*) during battery operation.[3,6]

In recent years, nanoscale aluminum oxide-based layers have been shown to act as low-cost but, at the same time, highly effective protective coatings on the CAM surface. Yet, the mechanism of protection is still not fully understood.[7–9] Regardless, it has been suggested, for example, that such coatings somewhat prevent transition-metal dissolution from the cathode, among others, by undergoing reaction with detrimental HF.[10]

Most often, a thin layer of Al_2O_3 is deposited onto the CAM *via* atomic layer deposition (ALD)[8,9] or by wet-chemistry routes.[7,11] ALD allows for uniform and conformal surface coating, however, at the expense of the need for complex equipment. ALD of Al_2O_3 is a well-established process, commonly comprising two half-reaction steps using trimethylaluminum (TMA) and H_2O as the reactants.[12,13]

Adopting the general ALD concept, in the present work, we made use of a facile solution-based process to prepare the protective shell on NCM811 by immersing powder material in a dilute solution containing TMA as the precursor. Since the reaction requires stoichiometric amounts of H_2O to form Al_2O_3 and to proceed efficiently, we took advantage of surface-adsorbed moisture, which is inherent in Ni-rich layered oxide CAMs. For a proof of concept, NCM811 with a H_2O content ranging from 1000 to 1200 ppm was employed. Such relatively wet CAM was dispersed in toluene, and then, TMA in toluene was added while stirring under an Ar atmosphere. Finally, the sample was recovered by filtration and washed two times with toluene, followed by drying in vacuum overnight (see experimental details in the ESI†). Karl-Fischer titration after TMA treatment revealed a H_2O content of <100 ppm. This finding confirms our hypothesis of TMA reacting with surface-adsorbed water species.

The Al content was determined by inductively coupled plasma-optical emission spectroscopy (ICP-OES) to be around 0.15 wt% (corresponding to a coating thickness of about 2 nm when assuming homogeneous coverage of secondary particles). Note that the Al content varies to some degree with the amount of adsorbed moisture. High-angle annular dark-field scanning transmission electron microscopy (HAADF-STEM) in combination with energy dispersive X-ray spectroscopy (EDX) also provided clear evidence of the presence of Al on the surface of NCM811 secondary particles (Fig. 1). However, the coating layer, which apparently consists of small-size Al-containing particles, was not uniform throughout with respect to both

[a] *Battery and Electrochemistry Laboratory, Institute of Nanotechnology, Karlsruhe Institute of Technology (KIT), Hermann-von-Helmholtz-Platz 1, 76344 Eggenstein-Leopoldshafen, Germany. E-mail: torsten.brezesinski@kit.edu*
[b] *BASF SE, Carl-Bosch-Str. 38, 67056 Ludwigshafen, Germany. E-mail: pascal.hartmann@basf.com*
[c] *Institute of Physical Chemistry & Center for Materials Research, Justus-Liebig-University Giessen, Heinrich-Buff-Ring 17, 35392 Giessen, Germany*

† Electronic supplementary information (ESI) available: Experimental details; rate performance data; differential capacity curves; Nyquist plots; and additional cycling data. See DOI: 10.1039/c8cc09618j

‡ These authors contributed equally.

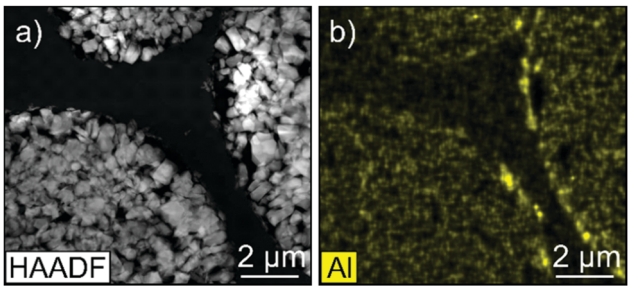

Fig. 1 (a) HAADF-STEM image of adjacent NCM811 secondary particles after TMA treatment and (b) the corresponding EDX map of Al.

thickness and degree of coverage. Furthermore, liquid-phase TMA treatment appeared to result in a different coating morphology than ALD. Nonetheless, this is not very surprising given that a self-limiting growth mechanism cannot be expected.

In analogy to ALD, we assume that the main species formed on the top surface of NCM811 is Al_2O_3. The presence of proton bearing species of the general formula $Al_xO_yH_z$ cannot be ruled out though. For reasons of simplicity, we refer to Al_2O_3 in the following.

The Al_2O_3-coated and uncoated (bare) NCM811 CAMs were electrochemically tested at 45 °C and at a rate of 1C in the voltage range between 2.8 and 4.2 V using single-layer pouch cells with a graphite anode. The areal loading was about 10 mg_{NCM811} cm^{-2}. Details about the electrode preparation, cell assembly and cycling conditions—including cell formation—can be found in the ESI.† Of note, the coating layer has very little effect on the cyclability (specific capacity, Coulombic efficiency, mean charge/discharge voltage) during the very first cycle (Fig. S1, ESI†). Fig. 2 shows the results from long-term cycling experiments after cell formation. Initial discharge capacities of 182–186 mA h $g_{NCM811}{}^{-1}$ were achieved for both the Al_2O_3-coated and bare NCM811 cells. All cells revealed an almost linear capacity decrease with increasing cycle number, and they were stopped after reaching 80% of their rated capacity. The latter is commonly defined as end-of-life. The bare NCM811 could be cycled for about 500 cycles, compared to 1100 cycles for the Al_2O_3-coated NCM811 (Fig. 2a). This result demonstrates that TMA treatment brings about considerable improvements in cycling stability. A similar trend can be deduced from the evolution of the mean discharge voltage with cycling (Fig. 2b). For the bare NCM811, the discharge voltage was relatively stable at slightly below 3.7 V during the first 100 cycles. However, with further cycling, it dropped quite significantly to about 3.5 V at the 500th cycle. In contrast, even after 1100 cycles, the mean discharge voltage was well above 3.5 V in the case of Al_2O_3-coated NCM811. This is also reflected in the rate performance, especially for C-rates $\geq$1C (Fig. S2, ESI†). During the initial rate capability test after 10 cycles, only slight differences in specific discharge capacity ($\leq$5 mA h $g_{NCM811}{}^{-1}$) were found between the Al_2O_3-coated and bare NCM811 CAM. However, already in the second test after 310 cycles there was a notable difference of up to 21 mA h $g_{NCM811}{}^{-1}$ at 3C rate. Likewise, cells using the Al_2O_3-coated NCM811 showed Coulombic efficiencies >99.95%,

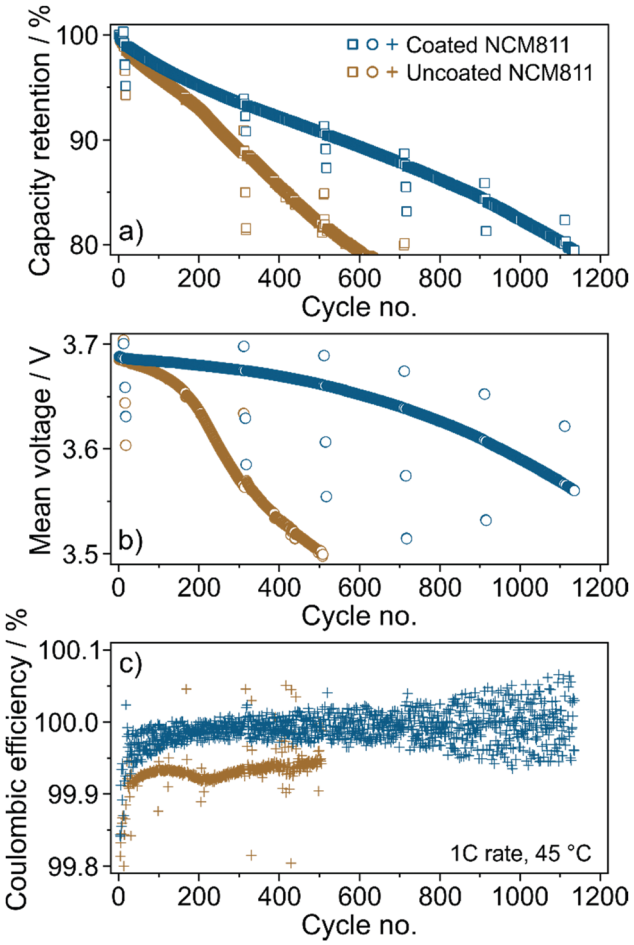

Fig. 2 Long-term cycling performance at 45 °C and 1C rate of single-layer pouch cells with a graphite anode using the Al_2O_3-coated and bare NCM811 CAM. (a) Discharge capacity retention, (b) mean discharge voltage and (c) Coulombic efficiency are shown *versus* the cycle number. "Deviating" data points are due to implemented rate capability tests during cycling (for details see the ESI†).

compared to 99.93 on average for the bare NCM811, thus indicating less side reactions after coating with Al_2O_3 (Fig. 2c).

As expected, almost identical charge/discharge curves in the initial cycles were obtained on cells using the Al_2O_3-coated and bare NCM811, with the voltage profile being characteristic of Ni-rich NCM CAMs (Fig. 3a and Fig. S1, ESI†). However, there were distinct differences in terms of capacity and overvoltage after 500 cycles (Fig. 3b). The usable specific discharge capacity of the Al_2O_3-coated and bare NCM811 cells was found to be 169 and 150 mA h $g_{NCM811}{}^{-1}$, respectively. The corresponding differential capacity plots indicated minor impedance build-up during cycling operation ($\ll$100 mV overvoltage with respect to the high-voltage features) when using the Al_2O_3-coated NCM811 (Fig. S3, ESI†). By contrast, the bare NCM811 CAM showed around two times higher overvoltage after the same number of cycles. In addition, some of the characteristic redox peaks vanished or merged with others.

In order to confirm that the decline in cell performance was mainly due to CAM degradation, electrochemical impedance

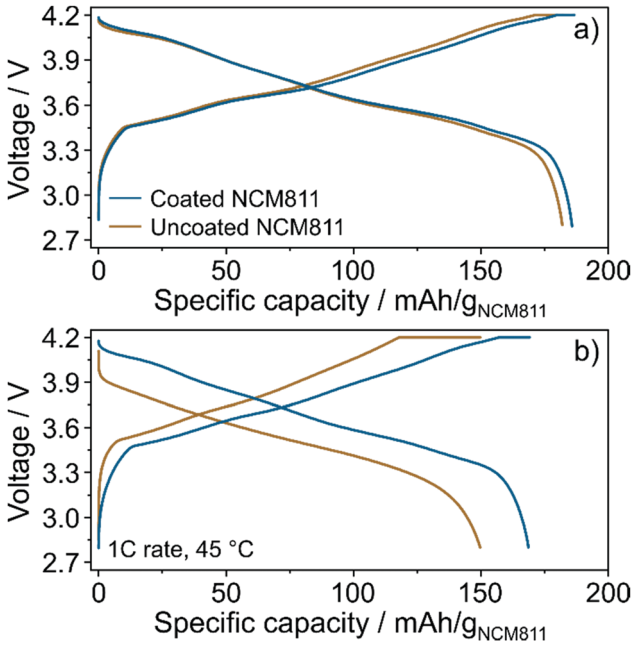

Fig. 3 Voltage profiles at 45 °C and 1C rate of single-layer pouch cells with a graphite anode using the Al_2O_3-coated and bare NCM811 CAM. For clarity, only the 2nd cycle after the cell formation (a) and the 500th cycle (b) are depicted.

spectroscopy (EIS) measurements were performed before cycling and after 1100 cycles (Fig. S4, ESI†). To this end, the pouch cells were opened in an Ar-filled glovebox and the electrodes were rinsed with dimethyl carbonate, dried and re-assembled in half-cells with a lithium metal counter-electrode. EIS data (Nyquist plots) obtained on the cycled graphite anode corroborated the expected increase in impedance. The first depressed semicircle in the high-frequency range (200 kHz to 1 kHz) increased presumably due to an increase in thickness of the solid electrolyte interphase (SEI) layer. The evolution of the second semicircle at medium frequencies (1 kHz to 10 mHz) indicated that the charge transfer resistance increased as well. However, the usable specific capacity was still close to the theoretical one (Fig. S4, ESI†), demonstrating minor degradation of the (bulk) graphite anode during long-term cycling.

EIS was also conducted on the NCM811 cathode. Again, the Nyquist plots revealed an impedance increase after cycling due to similar reasons as discussed above. The total increase was similar to that of the graphite anode. However, the usable specific capacity of NCM811 in half-cells was found to be relatively low (<130 mA h g_{NCM811}^{-1} at 25 °C and C/10 rate), thus suggesting that the overall capacity fade of full-cells can be addressed predominantly to CAM degradation, in agreement with literature.[14,15] Particle fracture (mechanical degradation), formation of rock salt-type phases (structural changes) and transition-metal dissolution (surface reactions), to name a few, are currently considered the main issues of Ni-rich layered oxide CAMs.[16,17]

Although Al_2O_3 surface coating of electrode material for different battery technologies has been intensively studied in the past,[3,7–11] we present here an innovative liquid-phase approach, leading to >100% improvement in cycling stability (*i.e.*, end-of-life) for a technologically relevant CAM. This is due to not only the presence of a protective shell, but also the decrease in H_2O content. Note that trace H_2O is detrimental to the cell cyclability (long-term performance *etc.*).[18,19] We also emphasize that no post-heating/annealing is required, which is both costly and time-consuming, especially in industrial fields. In addition, this excludes interdiffusion of Al species (Al^{3+}) into the CAM, resulting in doped samples or different chemically altered interfaces, as reported for $LiCoO_2$ and high-Ni NCMs.[7,20]

In summary, the aim of the current study was not to explore any new coating chemistry, but rather to simplify an established procedure. This was achieved by solvent-based synthesis at room temperature using highly reactive TMA as the precursor. Taken together, our approach combines two processing steps—usually considered indispensable before implementation of Ni-rich layered oxide CAMs in LIBs—namely drying and coating, at once. Thus, we believe that this simple and easily scalable process is of high interest to the battery community and may even pave the way toward development of a more general concept of surface coating.

This study is part of the projects being funded within the BASF International Network for Batteries and Electrochemistry. The authors thank Philipp Mueller (BASF SE) for TEM measurements.

Conflicts of interest

There are no conflicts to declare.

Notes and references

1 M. D. Radin, S. Hy, M. Sina, C. Fang, H. Liu, J. Vinckeviciute, M. Zhang, M. S. Wittingham, Y. S. Meng and A. Van der Ven, *Adv. Energy Mater.*, 2017, **7**, 1602888.
2 W. Liu, P. Oh, X. Liu, M.-J. Lee, W. Cho, S. Chae, Y. Kim and J. Cho, *Angew. Chem., Int. Ed.*, 2015, **54**, 4440–4457.
3 S.-T. Myung, F. Maglia, K.-J. Park, C. S. Yoon, P. Lamp, S.-J. Kim and Y.-K. Sun, *ACS Energy Lett.*, 2017, **2**, 196–223.
4 J. Kim, H. Lee, H. Cha, M. Yoon, M. Park and J. Cho, *Adv. Energy Mater.*, 2018, **8**, 1702028.
5 L. de Biasi, A. O. Kondrakov, H. Geßwein, T. Brezesinski, P. Hartmann and J. Janek, *J. Phys. Chem. C*, 2017, **121**, 26163–26171.
6 S. Neudeck, F. Walther, T. Bergfeldt, C. Suchomski, M. Rohnke, P. Hartmann, J. Janek and T. Brezesinski, *ACS Appl. Mater. Interfaces*, 2018, **10**, 20487–20498.
7 B. Han, T. Paulauskas, B. Key, C. Peebles, J. S. Park, R. F. Klie, J. T. Vaughey and F. Dogan, *ACS Appl. Mater. Interfaces*, 2017, **9**, 14769–14778.
8 A. M. Wise, C. Ban, J. N. Weker, S. Misra, A. S. Cavanagh, Z. Wu, Z. Li, M. S. Wittingham, K. Xu, S. M. George and M. F. Toney, *Chem. Mater.*, 2015, **27**, 6146–6154.
9 D. Mohanty, K. Dahlberg, D. M. King, L. A. David, A. S. Sefat, D. L. Wood, C. Daniel, S. Dhar, V. Majahan, M. Lee and F. Albano, *Sci. Rep.*, 2016, **6**, 26532.
10 S.-T. Myung, K. Izumi, S. Komaba, Y.-K. Sun, H. Yashiro and N. Kumagai, *Chem. Mater.*, 2005, **17**, 3695–3704.
11 A. Zhou, Q. Liu, Y. Wang, W. Wang, X. Yao, W. Hu, L. Zhang, X. Yu, J. Li and H. Li, *J. Mater. Chem. A*, 2017, **5**, 24361–24370.
12 R. L. Puurunen, *J. Appl. Phys.*, 2005, **97**, 121301.
13 S. M. George, *Chem. Rev.*, 2010, **110**, 111–131.
14 D. W. Abarbanel, K. J. Nelson and J. R. Dahn, *J. Electrochem. Soc.*, 2016, **163**, A522–A529.

15 K. J. Nelson, D. W. Abarbanel, J. Xia, Z. Lu and J. R. Dahn, *J. Electrochem. Soc.*, 2016, **163**, A272–A280.
16 A. O. Kondrakov, A. Schmidt, J. Xu, H. Geßwein, R. Mönig, P. Hartmann, H. Sommer, T. Brezesinski and J. Janek, *J. Phys. Chem. C*, 2017, **121**, 3286–3294.
17 A. O. Kondrakov, H. Geßwein, K. Galdina, L. de Biasi, V. Meded, E. O. Filatova, G. Schumacher, W. Wenzel, P. Hartmann, T. Brezesinski and J. Janek, *J. Phys. Chem. C*, 2017, **121**, 24381–24388.
18 J. Vetter, P. Novak, M. R. Wagner, C. Veit, K.-C. Möller, J. O. Besenhard, M. Winter, M. Wohlfahrt-Mehrens, C. Vogler and A. Hammouche, *J. Power Sources*, 2005, **147**, 269–281.
19 D. Aurbach, B. Markovsky, G. Salitra, E. Markevich, Y. Talyossef, M. Koltypin, L. Nazar, B. Ellis and D. Kovacheva, *J. Power Sources*, 2007, **165**, 491–499.
20 B. Han, B. Key, S. H. Lapidus, J. C. Garcia, H. Iddir, J. T. Vaughey and F. Dogan, *ACS Appl. Mater. Interfaces*, 2017, **9**, 41291–41302.